



ELSEVIER

Journal of Crystal Growth 242 (2002) 517–532

JOURNAL OF  
**CRYSTAL  
GROWTH**

www.elsevier.com/locate/jcrysgr

# Critical behaviour of the curved region near 111-facet edge of equilibrium shape cuprous selenide large single crystals

Jadranko Gladić\*, Zlatko Vučić, Davorin Lovrić

*Institute of Physics, Bijenička cesta 46, P.O. Box 304, HR-10000 Zagreb, Croatia*

Accepted 11 March 2002

Communicated by G. Muller

## Abstract

Several millimetres large spherical cuprous selenide single crystals with well developed (1 1 1) facets grown at about 30 K below the roughening temperature ( $T_R \approx 830$  K) and rapidly cooled to room temperature were used to test the universality and value of critical exponent describing the surface profile behaviour near the facet edge. Enlarged photographs (52.5 times) of part of the crystal profile were digitised with resulting spatial resolution of  $0.1904 \pm 0.0001 \mu\text{m}$ . After FFT low pass filtering, the position of crystal silhouette edge was determined as the loci of the extremes in the first derivative of each image row intensity profile. For assumed critical dependence  $z = A(x - x_0)^\theta$ , the inverse logarithmic derivative applied to crystal profile data points disclosed the extent of intervals of different behaviour, giving independently the respective indicative values of fitting parameters  $\theta$  and  $x_0$ . In three distinct regions non-linear Levenberg–Marquardt fitting was applied to original data sets.

In the region farthest away from the facet, the behaviour is well described by  $\theta \approx 2.5$  or by Andreev formula  $z = A(x_0 - x)^2 + B(x_0 - x)^4$ . In the stepped region, for  $\varphi = 13.98\text{--}17.12^\circ$  (tilt angle relative to facet plane), the critical exponent  $\theta = 1.499 \pm 0.003$  is found, in agreement with Pokrovsky–Talapov universality class predicted value of  $\theta = \frac{3}{2}$ . The step interaction energy, step free energy and facet free energy ratios obtained from data fitting parameters only, are compared to published values for  $^4\text{He}$ , Si and Pb single crystals.

The behaviour in the immediate vicinity of the facet edge is discussed in the light of dynamics features recently observed on different single crystals during growth (cuprous selenide,  $^4\text{He}$ ) and equilibration (Pb). © 2002 Elsevier Science B.V. All rights reserved.

PACS: 68.35.Mo; 81.10.Aj

Keywords: A1. Critical exponent; A1. Equilibrium crystal shape; A1. Pokrovsky–Talapov universality class; A2. Single crystal growth; B2. Superionic conductors

## 1. Introduction

There has been considerable interest in experimental investigation of the shape of equilibrium single crystals of various materials, in the temperature range where equilibrium crystal shape

\*Corresponding author. Tel.: +385-1-469-8888; fax: +385-1-469-8889.

E-mail addresses: gladic@ifs.hr (J. Gladić), vucic@ifs.hr (Z. Vučić), lovric@ifs.hr (D. Lovrić).

(ECS) comprises both planar facets and curved interfacial regions. Facets and curved regions join at edges, which can be either sharp or smooth. Within an  $xz$ -plane section of the crystal (perpendicular to the facet which is coplanar with the  $xy$  facet plane), the shape of curved interface in the vicinity of a smooth edge positioned at  $(x_0, 0)$  is described as [1,2]

$$z = A(x - x_0)^\theta + \text{higher order terms.} \quad (1)$$

The main objective of the experimental endeavour has been to test the universality and value of the critical exponent  $\theta$ , theoretically predicted to be equal to  $\frac{3}{2}$ .

The ECS materials investigated thus far have been mostly metals, with single crystals up to 10  $\mu\text{m}$  in diameter, on graphite substrate (Pb [1,3–5], Au [3,6,7], In [8–10].) The shape of 9  $\mu\text{m}$  Pb crystal [1] is described with  $\theta = 1.60 \pm 0.15$  within a curved surface region not extending all the way to the edge (latest STM measurement on a few  $\mu\text{m}$  large Pb crystals [5] at 380 K give  $\theta = 1.49 \pm 0.06$  independent of azimuth); the shape of 4  $\mu\text{m}$  In crystals with  $\theta \approx 2$  close to the edge and  $\theta \approx 1.60 \pm 0.10$  further away, while for describing a few  $\mu\text{m}$  large Au crystals having sharp edges [9] a term linear in  $(x - x_0)$  was used [3]. Profiles of 0.36–7.2  $\mu\text{m}$  Si crystallites [11] (equilibrated apexes of small silicon columns on silicon substrate) are described with  $\theta = 1.5$  (with a 6% uncertainty) for misorientation of profile from the facet between  $3^\circ$  and  $17^\circ$ .

The theory describes the shape of idealized large crystals in the thermodynamic limit ( $V \rightarrow \infty$ , at fixed  $T$ , where the atomic scale details of crystal outline effectively disappear), with the mathematically sharp features such as strict planarity of facets, the sharpness of edges and corners, etc. The discrepancy between these and the experimentally observed features are expected to be more pronounced for smaller crystals (their size being limited by the equilibration time).

The investigated  $^4\text{He}$  single crystals [12–14] were a few millimetres large and their shape was described [12] with  $\theta = 1.55 \pm 0.06$ , starting at the facet edge. On millimetre size growing single crystals of ordinary  $\text{H}_2\text{O}$  ice [15], the value of  $\theta =$

1.74 was obtained, again fitted over the entire rounded profile, from the very facet edge.

The aim of this article is to investigate the shape of the curved region near the (1 1 1) facet edge of an equilibrium shape large spherical single crystal of cuprous selenide. Cuprous selenide  $\text{Cu}_{2-x}\text{Se}$  is a representative of a group of chemically and structurally simplest superionic conductors, namely metal chalcogenides ( $\text{M}_{2\pm x}\text{Ch}$ ,  $\text{M} = \text{Ag}, \text{Cu}$ ;  $\text{Ch} = \text{S}, \text{Se}, \text{Te}$ ). These materials exhibit large ionic and electronic conductivity, thus enabling fast bulk metal atom transport, while still in solid phase. They have only recently been introduced as convenient materials for studying ECS properties [16–20], since they are, besides the solid  $^4\text{He}$  single crystals, the only materials having large (sub-centimetre) size crystals of apparently ECS form that can be grown on a practical time scale (of several days).

### 1.1. Theoretical background

Let us briefly review the underlying theory and basic definitions of the ECS along the lines set forth by Landau [21] and Jayaprakash et al. [2].

As crystals are anisotropic, the equilibrium shape of a crystal is the direct consequence of the surface free energy per unit area  $f(\vec{h})$  dependence on the crystal surface (described by  $z(x, y)$ ,  $\vec{h} = \vec{\nabla}z(x, y)$ , origin at the crystal centre) orientation relative to crystallographic axes, at given temperature. The shape is determined [2,21] by minimization of the surface free energy, subject to the constant volume constraint, i.e. by minimization of

$$\int dx dy [f(\vec{h}) - 2\lambda z(x, y)], \quad (2)$$

where  $\lambda$  is the Lagrange multiplier. The solution to this variational problem is not strictly valid [22] except in the thermodynamic limit  $V \rightarrow \infty$ , since by writing the total free energy in the form of Eq. (2) the physical effects of atomic scale details (e.g. edge and corner energies, curvature corrections, and the like) responsible for finite size corrections are omitted.

As pointed out by Rottman et al. [1], the prediction of critical exponent  $\theta = \frac{3}{2}$  is based on

two propositions: (i) that interface can be modelled as a two-dimensional (2D) surface (for small bulk correlation length), and (ii) that the dominant excitations of such surface are “steps” or “ledges” (TSK—terrace–step–kink model).

Microscopically, the transition region with surface orientations arbitrarily close to a high-symmetry direction (flat facet—smooth phase), the so-called vicinal surfaces, can be viewed as a sequence of atomically smooth terraces separated by steps of height  $a$  (lattice plane spacing) and spacing  $l$ . The angle  $\varphi$  between the vicinal surface and the facet is proportional to the linear density of steps  $1/l$  ( $\varphi \sim \tan \varphi \sim a/l = |\vec{h}|$ ). It should be stressed that such a picture is valid only if the tilt angle  $\varphi$  is small enough [23,24]. On such stepped surface, the distance between steps is large and the steps are well defined. If the angle  $\varphi$  gets too large, the terrace width becomes comparable to step width—thus the regular staircase disappears and the surface becomes rough.

Generally, the surface free energy per unit area for the stepped surface can be written as an expansion [3] in terms of moduli of  $\vec{h}$ :

$$f(\vec{h}) = \beta_0 + \beta_1|\vec{h}| + \beta_2h^2 + \beta_3|\vec{h}|^3 + \dots \quad (3)$$

with generally temperature dependent coefficients  $\beta_n$ . The term  $\beta_0$  is the surface free energy per unit area of the facet ( $\vec{h} = 0$ ),  $\beta_1|\vec{h}|$  corresponds to the step free energy that vanishes at the roughening transition. The higher order terms represent interactions between steps.

A “very particular choice” [3] of coefficients in Eq. (3) (in the framework of the mean-field theory) gives the Andreev [25] crystal shape (in  $xz$ -plane, as in Eq. (1)) of the form

$$\lambda z(x) = z_0 + a(\lambda x)^2 + b(\lambda x)^4. \quad (4)$$

Models [2] taking into account thermal fluctuations in step positions, which exclude voids and overhangs (solid-on-solid condition), with only repulsive interactions between steps, give the free energy dependence on slope  $\vec{h}$  of the stepped surface

$$f(|\vec{h}|) = \beta_0 + \beta_1|\vec{h}| + \beta_3|\vec{h}|^3. \quad (5)$$

The resulting crystal shape in the vicinity of facet edge is described by the power law depen-

dence [2] (again in  $xz$ -plane):

$$\lambda z(x) = \begin{cases} \beta_0 & \text{for } |\lambda x| < \beta_1, \\ \beta_0 - \frac{2}{3^{3/2}\beta_3^{1/2}}(|\lambda x| - \beta_1)^{3/2} & \text{for } |\lambda x| \geq \beta_1. \end{cases} \quad (6)$$

The exponent  $\theta = \frac{3}{2}$  (critical exponent) describing the shape of the curved surface, characterises such a transition (second-order phase transition) as belonging to the Pokrovsky–Talapov [26] (or Gruber–Mullins [27]) universality class. Such universal exponent should be independent of the observed material, orientation of facet or azimuthal angle of the  $xz$ -plane crystal section.

The paper is organised as follows.

In Section 2 we review the preparation of large spherical cuprous selenide single crystals with well developed (111) facets. The methods of noise removal and determination of crystal silhouette edge position on digitised enlarged photographs of part of crystal profile (the facet and adjacent curved region) are discussed.

In Section 3 the detailed analysis of functional dependence of thus obtained crystal profile data points is given. For assumed critical dependence  $z = A(x - x_0)^\theta$ , the inverse logarithmic derivative approach is used to disclose the intervals of different behaviour and to obtain indicative values of fitting parameters  $\theta$  and  $x_0$  independently.

The results are discussed in Section 4. The value of scaling parameter  $\lambda$  is estimated in order to calculate the  $\beta_0$ ,  $\beta_1$  and  $\beta_3$  coefficients, while the ratios of these coefficients are obtained from the fitting parameters (of the critical behaviour in the stepped region) only. These are compared with values obtained by other authors on  $^4\text{He}$ , Si and Pb single crystals. The extent of the stepped region and the possible origin of the behaviour of crystal profile adjacent to the facet edge is discussed.

## 2. Experimental procedure

The method of growth [19,20] of superionic conductor cuprous selenide  $\text{Cu}_{2-x}\text{Se}$  single crystals in a solid/vapour system is based upon the fast bulk Cu atoms transport at temperatures from

300 K up to the melting temperature  $T_m = 1450$  K. The crystals are grown using modified Ohachi's method [17,18], around the tip of a quartz capillary (the tip being  $<10\%$  of the crystal sphere volume, see Fig. 4 in Ref. [19]). The tip narrowing is used for single crystal seed selection, and for keeping the current density of Cu atoms smaller [20] ( $10^3$ – $10^5$  times) than the one of selenium molecules. Thus high quality spherical single crystals are grown in the solid-state crystallisation mode [28,29], with constant volume growth rate ( $0.1$ – $0.9$  mm<sup>3</sup> h<sup>-1</sup>) [19,20].

The partly faceted (circular (111) facets) and partly rounded crystals were grown at about 30 K below the roughening temperature,  $T_R \approx 830$  K, for several days, until reaching several millimetres in diameter. The growth was observed in situ, measuring simultaneously facet and sphere radii. Their ratio, characterising the crystal shape, shows the exponential-like relaxation (with relaxation time constant  $\tau \sim 1200$  min, see Fig. 6. in Ref. [20]) towards the equilibrium value with time, as radial growth rate decreases (from 350 to 1.5 nm s<sup>-1</sup>), all the time obeying volume vs. time linearity. Then they were quickly cooled (from 800 to 600 K in less than a minute) to room temperature (hopefully without changing their shape and quality). The single crystals with well-developed eight (111) facets (with relative orientations perfectly reflecting the point group symmetry of FCC crystal), thus grown and quenched, were used to obtain the enlarged photographs of the crystal edge projection. Their growth shape is believed to be as near to equilibrium shape as practically attainable (the exponential approach to equilibrium becoming prohibitively slow after growth time  $> 5\tau$ ).

A halogen point-like white light source and a convergent lens provided a parallel light beam for backlighting the crystal. The part of crystal with a facet was brought into the centre of the light beam, with the facet surface parallel to paraxial rays. Another lens was used to obtain a magnified picture of the facet and its neighbourhood silhouette projected directly on photographic paper (ILFORD black and white Ilfobrom FB IB3.1P). A continuous coloured glass filter was used to provide monochrome illumination, thus reducing

chromatic aberrations. The exposure time was about 20 min.

By projecting standard calibration grid several times larger than the single crystal samples (DRC Metrigraphics,  $10 \times 3$  mm,  $40 \mu\text{m}$  bars) a smaller area (approx.  $30 \times 30$  cm) with no pincushion distortions was determined in the image centre. Subsequently, the observed single crystal was placed so as to get the image of facet and its neighbourhood well within this area. Testing on standard steel balls (comparable in size with our single crystals) using a CALCOMP digitising board to obtain coordinates of their silhouette edge from photographs, proved that within the chosen central area there were no detectable image distortions (the fit standard deviations were at the worst 10 times smaller than the declared deviation of standard balls' radii, at a given magnification of about 53 times).

The photographs of single crystal facet edge area were digitised using a professional drum scanner (Linotype-Hell Cromagraph S3700, sampling aperture  $12 \mu\text{m}$ , resolution  $100$  dots mm<sup>-1</sup>), thus avoiding the subjective choice of crystal projection edge points sampled when using a digitising board. A typical scan of a crystal photograph (crystal with  $2R = 7.80 \pm 0.05$  mm, measured with vernier calliper) resulted in non-compressed RAW file of 26710 rows with 5499 pixels each (Fig. 1).

Due to the initial orientation of the photograph with edge extending roughly along the  $y$ -direction, i.e. perpendicular to the pixel rows, a basically one-dimensional (1D) approach to the edge detection problem at hand proved to be quite appropriate.

Fig. 2 shows part of a typical row taken from the middle part of the image, crossing the crystal edge near the facet end. The white part (crystal) has a uniform grey level value of 255, while the "black" background has a grey value of  $40 \pm 20$ , with superimposed noise. The transition area defining the crystal silhouette outline shows a gradual change from white to "black" over typically  $120 \pm 20$  pixels, with the similar high-frequency noise. In order to get an objective edge position within a row, a smoothing filter matching the known requirements of biological vision



Fig. 1. (111) facet and its neighbourhood projected directly on photographic paper (rotated 90° counter-clockwise, magnification  $52.51 \pm 0.03$  times, digitised with 2540 dpi, 255 grey levels, image size  $5499 \times 26710$  pixels). The resolution obtained is  $0.1904 \pm 0.0001 \mu\text{m}$ . The row of pixels analysed in Fig. 2 is indicated by dashed line.

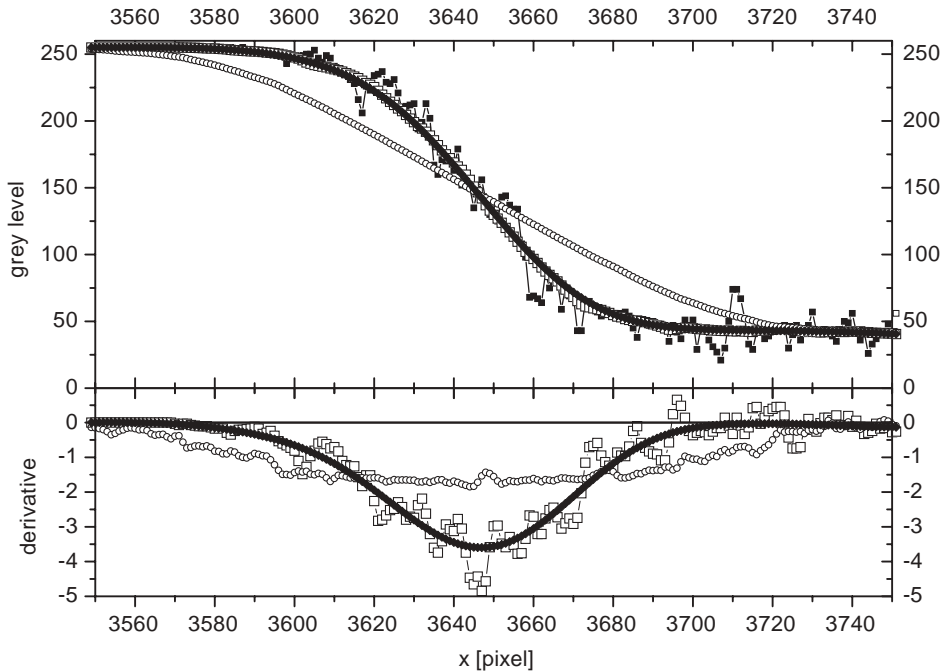


Fig. 2. (a) A part of intensity profile of a row of pixels (indicated in Fig. 1) crossing the crystal silhouette edge: original data—■; smoothed by adjacent averaging (window width of 29 pixels—□, 125 pixels—○); smoothed by FFT low pass filtering—◆ (frequency filtering window width was 29); (b) numerical derivatives of the smoothed intensity profile curves from (a). The minimum of derivative corresponds to the crystal silhouette edge position in the given row. Only the FFT smoothed intensity data result in well-defined single minimum.

(smooth and localised in spatial, and band limited in the frequency domain [30]) should be applied first. The edge position is then determined as the locus of the extreme of the numerical derivative of row intensity profile.

1-D FFT smoothing (low pass filtering) was applied to each pixel row of the image [31]. FFT smoothed grey-level data with frequency filtering window of width 29 (removing all oscillations in real space of periodicity shorter than 29 pixels)

have a smooth first derivative with well-defined single minimum, in contrast to the derivative of adjacent average smoothed data with a spatial domain window of 29 points (Fig. 2(b)). For smaller window widths, the position of the minimum for a given row shifts significantly, and the spread in values for consecutive image rows is large (100–40 pixels). For larger window widths the position of the edge for each row approaches a stable value (not changing with further enlarging

the window), with positions of minima in consecutive rows differing at most by several pixels. When 2-D FFT smoothing was applied to the whole image matrix, independently varying  $x$ - and  $y$ -window widths, the position of the edge proved to be almost completely insensitive to  $y$ -filtering, as expected due to the original orientation of edge in the photograph. However, 2-D filtering with the same  $x$ - and  $y$ -filtering window widths (large enough to give a stable value of the edge position in a given row) removed all local extremely large amplitude grey level oscillations (e.g. an erroneous several pixels large white spot on “black” background). The working width of the filtering window (for both spatial directions) was chosen to be in the range from 91 to 111.

Thus obtained  $x$  and  $y$  coordinates of the edge were then interchanged in order to obtain the data plot in which the facet direction was roughly parallel to the  $x$ -axis.

### 3. Data analysis and results

In order to comply with the functional dependence  $z(x)$  describing the shape of the curved ECS interface profile in the vicinity of a facet (Eq. (1),  $x$ -axis coincident with facet) and avoid unnecessary additive constants, we had to determine the reference facet line first.

The parameters of the linear regression fit  $z_i = A + Bx_i$ , obtained by the least-squares method (over  $i = 2841$  facet profile data points starting somewhat within the facet, to avoid the influence of the points near the edge) are

$$A = 6362.0 \pm 0.7, \quad B = -0.09431 \pm 0.00005, \\ \sigma = 2.47532.$$

Fig. 3 shows the linear fit through the  $\sim 0.5$  mm of the facet (facet diameter  $d \approx 1.38$  mm), together with the residual points showing that the scattering of data points around the reference facet line is within at most  $\pm 10$  pixels, i.e.  $\pm 2 \mu\text{m}$  (this being the intrinsic scattering of the crystal projection outline data). The crystal profile plot was afterwards rotated using the slope value ( $B = \tan \phi$ ), then translated to make the facet coincident with the  $x$ -axis, and finally reflected about the  $x$ -axis.

The resulting plot is shown in Fig. 4. The small inset shows the part of the crystal profile obtained from the scanned photograph as a part of an idealized spherical crystal coinciding with the profile in regions far away from the facet.

It proved more advantageous to apply the following fitting procedure to the scanned profile left of the facet in Fig. 4, since it extends further away from the facet edge than the corresponding right-side part. (The tilt angle  $\varphi$  between the curved surface and the facet extends up to  $\approx 28^\circ$ , being equivalent to the polar angle  $\omega$ , measured from the facet centre normal, of  $\approx 45^\circ$ .)

In compliance with Eq. (1), we want to fit the crystal shape profile in the vicinity of the facet to the functional form with three fitting parameters:

$$z = A(x_0 - x)^\theta, \quad (7)$$

where  $x_0$  is the facet edge position, and  $\theta$  is the critical exponent. The large number of data points and their homogeneous density in both  $x$  and  $z$  directions over the whole photograph permit us to circumvent the tedious trial-and-error procedure of determining the interval within which functional form (7) is applicable, by making use of the following procedure.

Taking the logarithm of Eq. (7) we have  $\ln z = \ln A + \theta \ln(x_0 - x)$ . The inverse of the derivative of  $\ln z$  is

$$\left[ \frac{d(\ln z)}{dx} \right]^{-1} = -\frac{x_0}{\theta} + \frac{1}{\theta}x$$

being linear in  $x$ . Thus, transforming the original (rotated, translated and reflected) data and plotting them as  $[d(\ln z)/dx]^{-1}$  vs.  $x$  should give a straight line in an interval where they are appropriately described by the critical dependence given by Eq. (7). The least-squares linear fit parameters in thus (visually) disclosed intervals give independently the corresponding values of the critical exponent  $\theta$ , and the facet edge position  $x_0$ .

It should be kept in mind that the particular steps involved (numerical differentiating of  $\ln z$ , taking inverse) greatly amplify the inherent noisiness of the original data set, but this proves to be only visually distracting for the intended purpose. In order to diminish the scattering, which obscures

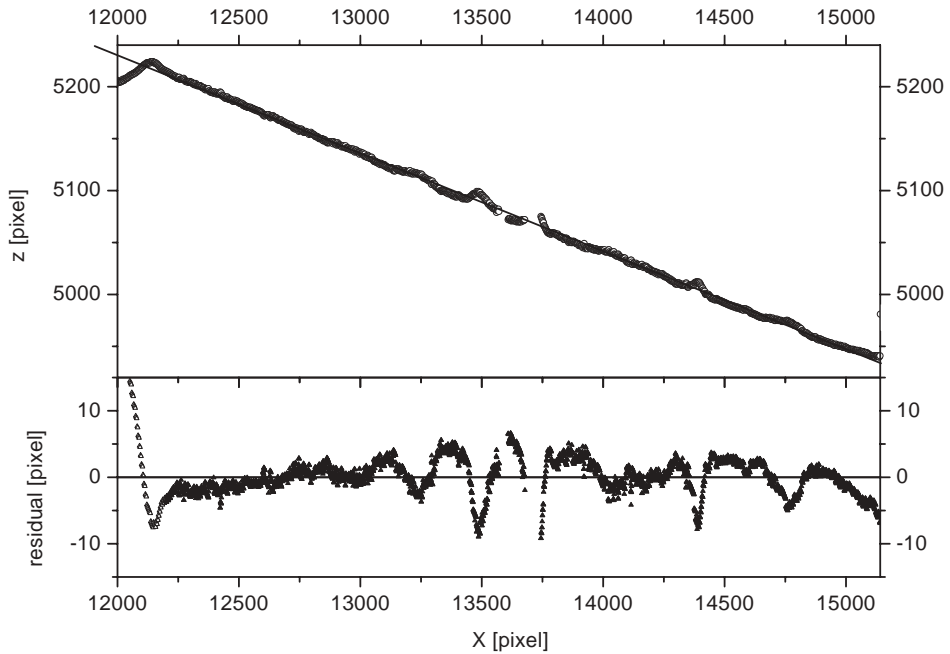


Fig. 3. Least-squares linear regression fit  $z_i = A + Bx_i$  over 2841 facet data points ( $\sim 0.5$  mm of the facet). The residue plot ( $\sigma = 2.47532$ ) shows that the intrinsic scattering of data points is at most  $\pm 10$  pixels (i.e.  $\pm 1.9 \mu\text{m}$ ).

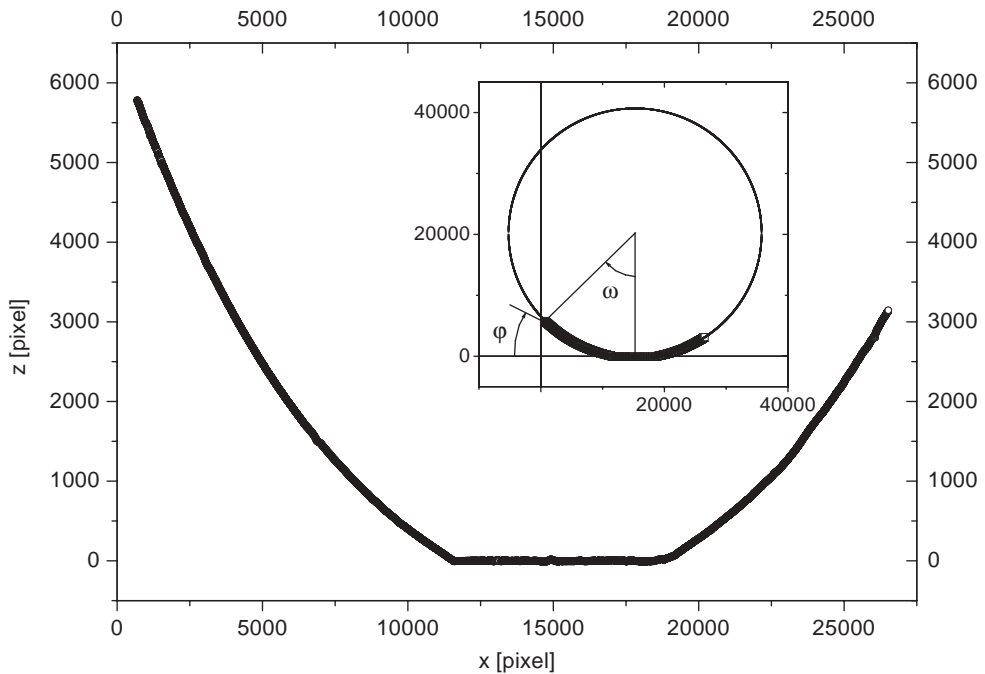


Fig. 4. Crystal profile data obtained from the photograph in Fig. 1, in the coordinate frame having  $x$ -axis coincident with the facet. *Inset*: The same data shown as part of an idealised spherical crystal coinciding with the profile in curved regions far away from the facet. On the left side, the profile data extend up to tilt angle  $\varphi \approx 28^\circ$  (corresponding to the polar angle  $\omega \approx 45^\circ$ ).

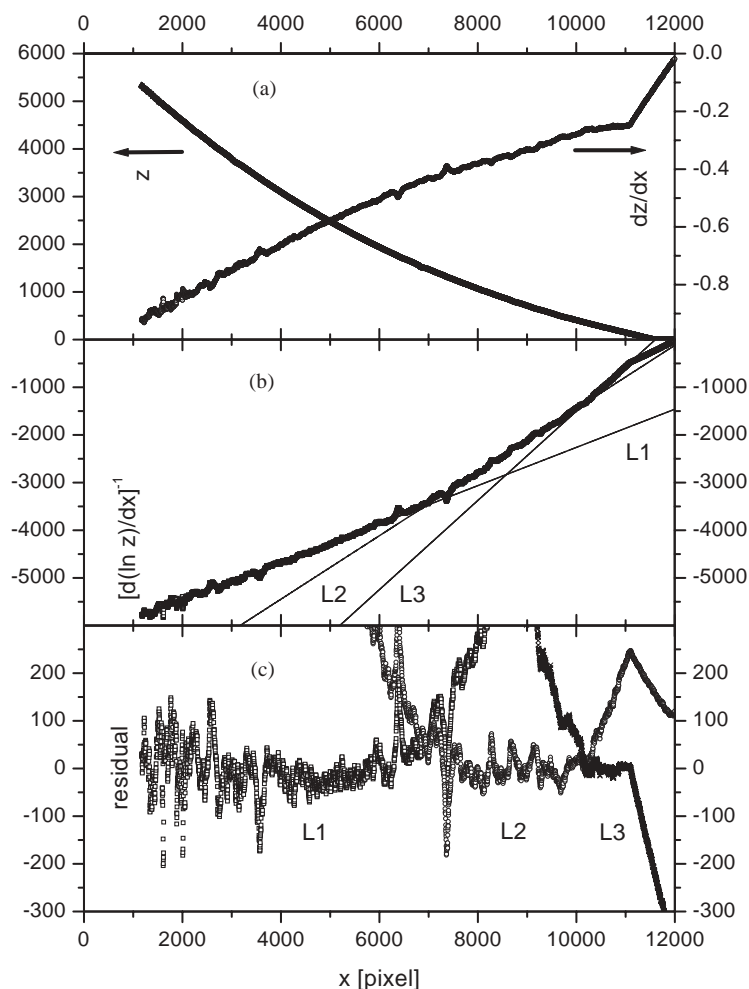


Fig. 5. Application of inverse logarithmic derivative to crystal shape profile data, in order to determine the intervals of applicability of  $z = A(x_0 - x)^\theta$  dependence. (a) Crystal profile data left of facet smoothed by moving averaging over 1024 adjacent points, and the numeric first derivative. (The linear segment at far right is artificial, coming from zero-value facet points included in the averaging interval.); (b) Three distinct linear segments of the inverse logarithmic derivative, giving three sets of independently determined parameters  $x_0$ ,  $\theta$ . (c) The residual values of the linear fits in (b) clearly showing the extent of respective intervals.

the general data trends, we first applied smoothing by moving averaging over  $N$  adjacent points of the original data set, and only after that proceeded with the inverse logarithmic derivative approach. The obtained values of  $\theta$  and  $x_0$  are quite insensitive to the adjacent averaging interval ( $N = 64, 128, 256, 512$  or  $1024$ ), the only effect of averaging being the artificial linear segment of the  $dz/dx$  and  $[d(\ln z)/dx]^{-1}$  plots at the right-hand side of the plot (Fig. 5), due to facet points (with

ordinates  $\approx 0$ ) being included in the adjacent average smoothing.

The resulting  $z$ ,  $dz/dx$  and  $[d(\ln z)/dx]^{-1}$  vs.  $x$  plots are shown in Fig. 5.

In Fig. 5(b) the existence of three distinct linear segments of the  $[d(\ln z)/dx]^{-1}$  plot, having different slopes and intercept values is clearly visible (besides the artificial linear segment closest to the facet edge). The residual values of the linear fits to three different segments shown in Fig. 5(c),

confirm the appropriateness of different sets of parameters in these three intervals. Assuming for the moment that there are indeed three adjacent regions of the crystal surface profile near the facet the shape of which can be described by critical dependence, we obtain the values shown in Table 1.

In order to check these indicative results, we applied the non-linear Levenberg–Marquardt [31] fitting of functional dependence (7) to the original data sets in the same intervals. Thus obtained values are shown in the last column of Table 1 (being almost the same as those obtained from the linear fits of the inverse logarithmic derivative).

In the region farthest away from the facet (from  $\varphi = 17.96\text{--}27.09^\circ$ ), we tried to describe the crystal profile shape by fitting the data points to a circle,  $z = z_c \pm \sqrt{R^2 - (x_c - x)^2}$  (shown in Fig. 6), obtaining

$$R = 20480 \pm 12, \quad x_c = 15255 \pm 7, \\ z_c = 20208 \pm 10, \quad \chi^2 = 20.94905.$$

Comparing these values to the crystal diameter measured with a vernier calliper in the rounded region between the facets,  $2R = 7.80 \pm 0.05$  mm, the magnification of the photograph is  $52.51 \pm 0.03$ , and thus the distance between two adjacent image pixels corresponds to  $0.1904 \pm 0.0001 \mu\text{m}$  on the single crystal sample. All of the following results were transformed to millimetres scale using this correspondence. The thus obtained values for circle radius and centre:

$$R = 3.900 \pm 0.002 \text{ mm}, \quad x_c = 2.905 \pm 0.001 \text{ mm}, \\ z_c = 3.848 \pm 0.002 \text{ mm}, \quad \chi^2 = 0.00399$$

are used afterwards as the ones describing the position of the centre (the Wulff centre) of our crystal (in calculating the angular extent of particular fitting intervals, and determining the values of  $\beta_n$  coefficients).

This method of determining the Wulff centre of our crystal was used since it was not possible to obtain the undistorted projection of the whole crystal silhouette with the same magnification/resolution. However, as our crystals are almost spherical, grown without spatial constraints (except the discussed capillary tip) and of FCC

Table 1  
Summary of the fitting parameters in distinct intervals of the crystal shape profile

	$x_c - x$ (mm) range	$z_c - z$ (mm) range	$\varphi$ range	$-\omega$ range	$[d(\ln y)/dx]^{-1}$ vs. $x$ plot parameters	Data fitting parameters $z = A(x_0 - x)^2 + B(x_0 - x)^4$
Facet	$-0.6934$ $0.6934$	$3.8484$ $3.8484$		$10.21$ to $-10.21^\circ$ $\Delta\omega = 20.43^\circ$		
	$0.7913$ $0.9626$	$3.8262$ $3.7827$	$13.11\text{--}13.84^\circ$ $\Delta\varphi = 0.74^\circ$	$11.68\text{--}14.28^\circ$ $\Delta\omega = 2.59^\circ$	$\theta = 1.069$ $x_c - x_0 = 0.6947 \text{ mm}$	$A = 0.27 \pm 0.01 \text{ mm}^{-1-0}$ $\theta = 1.082 \pm 0.004$ $x_c - x_0 = 0.6913 \pm 0.0008 \text{ mm}$ $\chi^2 = 0.00023$
Stepped	$0.9816$ $1.4767$	$3.7773$ $3.6080$	$13.98\text{--}17.12^\circ$ $\Delta\varphi = 3.13^\circ$	$14.57\text{--}22.26^\circ$ $\Delta\omega = 7.69^\circ$	$\theta = 1.502$ $x_c - x_0 = 0.5854 \text{ mm}$	$A = 0.287 \pm 0.007 \text{ mm}^{-1-0}$ $\theta = 1.499 \pm 0.003$ $x_c - x_0 = 0.5882 \pm 0.001 \text{ mm}$ $\chi^2 = 0.00132$
	$1.6101$ $2.7728$	$3.5522$ $2.7470$	$17.96\text{--}27.94^\circ$ $\Delta\varphi = 9.98^\circ$	$24.38\text{--}45.27^\circ$ $\Delta\omega = 20.89^\circ$	$\theta = 2.495$ $x_c - x_0 = -0.074 \text{ mm}$	$A = 0.1450 \pm 0.0002 \text{ mm}^{-1}$ $B = 0.0003486 \pm 0.000007 \text{ mm}^{-3}$ $x_c - x_0 = 0.2118 \pm 0.0004 \text{ mm}$ $\chi^2 = 0.0041$

Note that the profile data have been transformed to millimetres (5252 pixels  $\leftrightarrow$  1 mm) and the geometrical values are expressed with respect to the centre ( $x_c, z_c$ ) of the idealised spherical crystal coinciding with the profile in curved region furthest away from the facet (see Figs. 4 and 6).

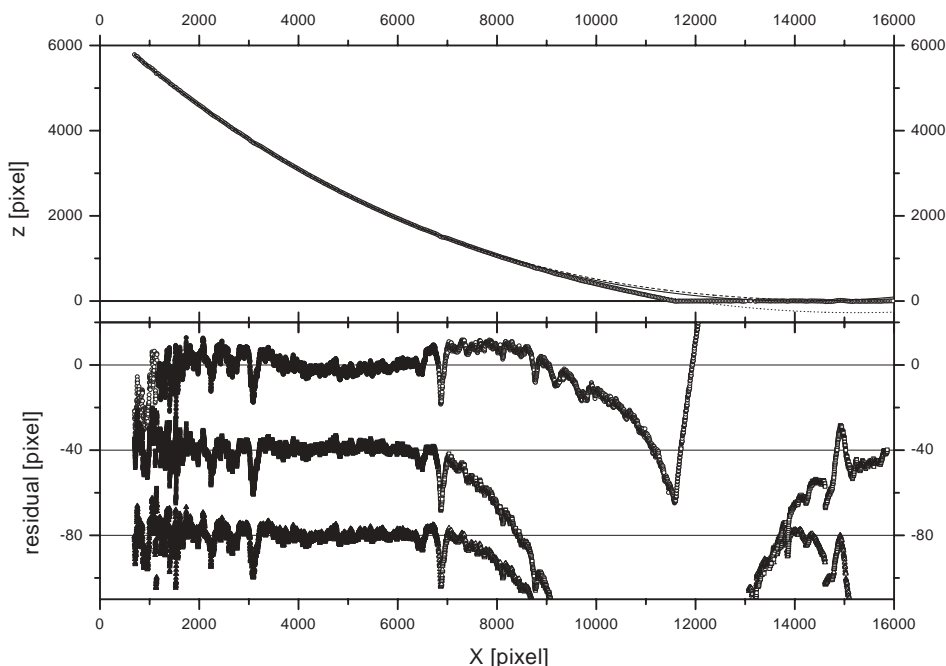


Fig. 6. Non-linear fits of the crystal profile data (5252 pixels  $\leftrightarrow$  1 mm) in the region farthest away from the facet, together with residue plots to a circle  $z = z_c \pm \sqrt{R^2 - (x_c - x)^2}$ ,  $\chi^2 = 20.94905$  (dotted line;  $\circ$ ), to critical dependence  $z = A(x_0 - x)^\theta$ ,  $\theta = 2.538 \pm 0.002$ ,  $\chi^2 = 16.67726$  (dashed line;  $\square$ ), to the Andreev formula  $z = A(x_0 - x)^2 + B(x_0 - x)^4$ ,  $\chi^2 = 21.29286$  (full line;  $\triangle$ ). The symbols in the residue plot within the fitting interval are filled. The residue plots  $\square$  and  $\triangle$  are shifted for  $-40$  and  $-80$  pixels, respectively.

symmetry (as confirmed by relative orientations of eight present (111) circular facets), it seems justifiable to identify the circle fit centre with the Wulff centre position (the fit is equally good on both sides of the facet, in corresponding intervals). To further test this claim, a circle was constructed directly on the photograph, enclosing everywhere the visible part of crystal edge projection. Thus obtained value of crystal radius, compared to the direct measurement of crystal diameter by a vernier calliper gives the magnification of  $52.5 \pm 0.1$  times, and therefore the crystal radius value of  $20475 \pm 40$  pixels. This is practically equal to the value obtained from fit to a circle (within its error margin) which is, strictly speaking, the local radius of surface curvature within the fit interval. The fact that our crystals are of spherical shape was also confirmed in testing the volume vs. time linearity during the crystal growth [19], where the crystal radius was measured as the radius of

maximum circular envelope of the sphere projection on screen (between the opposite rounded parts of surface in regions between facets) [20].

The facet itself covers the angular range of  $\Delta\omega \approx 20.43^\circ$  (as viewed from the centre  $(x_c, z_c)$  of the circle).

Fig. 7 shows the fit of the original data to the critical dependence (7), with  $\theta = 1.499 \pm 0.003$  and the residue plot. The fit describes the crystal shape quite well within the angular range  $\Delta\varphi = 3.13^\circ$  (from  $13.98^\circ$  to  $17.12^\circ$ ), the critical exponent disclosing it as the true stepped region. However, this dependence obviously does not seem to be appropriate for describing the crystal profile in the closest neighbourhood of the facet edge.

In the region further away from the facet (the same interval as for fit to a circle), beyond the extent of the stepped region, the critical dependence indicated by the inverse logarithmic derivative plot would be characterised by

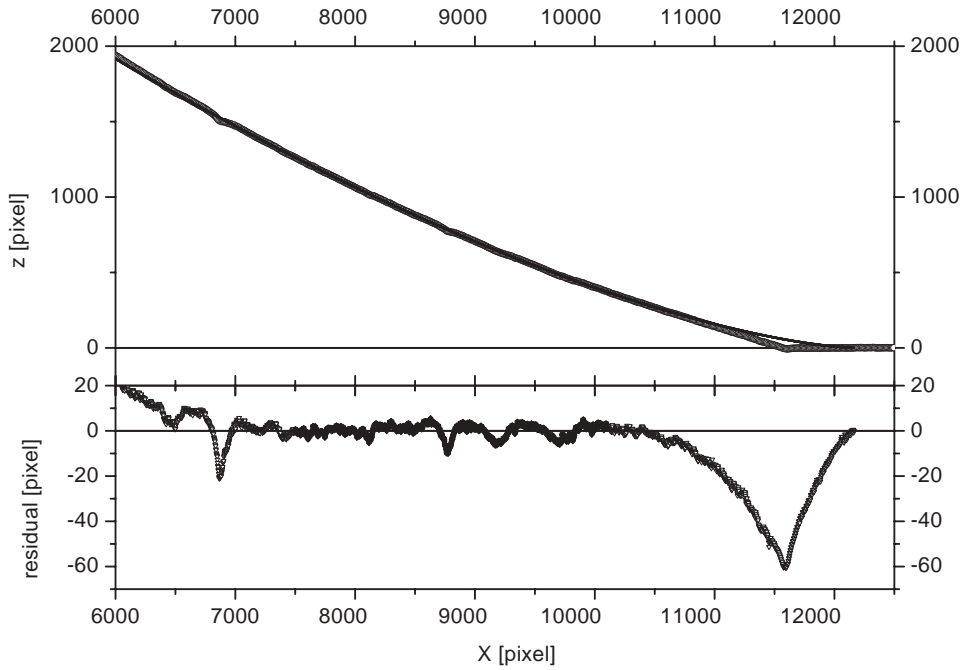


Fig. 7. Non-linear fit of the crystal profile data to critical dependence  $z = A(x_0 - x)^\theta$  in the stepped region,  $\theta = 1.499 \pm 0.003$ ,  $\chi^2 = 6.90725$ . The symbols in the residue plot within the fitting interval are filled.

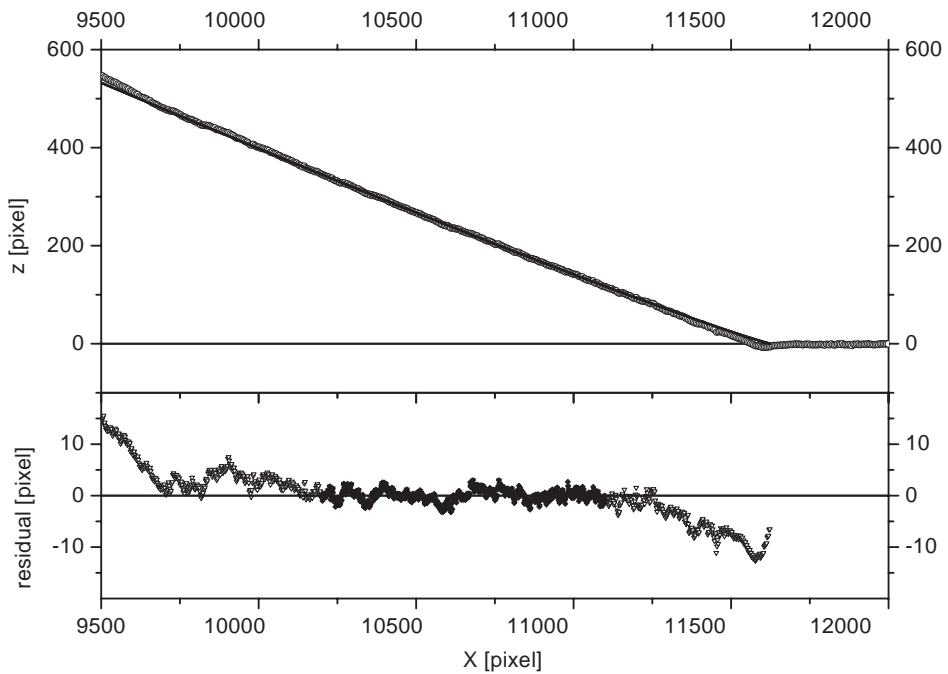


Fig. 8. Non-linear fit of the crystal profile data to critical dependence  $z = A(x_0 - x)^\theta$  in the region adjacent to the facet edge,  $\theta = 1.082 \pm 0.004$ ,  $\chi^2 = 1.23$ . The symbols in the residue plot within the fitting interval are filled.

$\theta = 2.538 \pm 0.002$  obtained from fitting the original data (Fig. 6). As such dependence has not been mentioned in the existing literature, and this is the interval where the surface is rough and TSK model is no longer applicable, we managed to fit the data in this interval quite well (Fig. 6) to the Andreev [25] (mean-field) formula:

$$z = A(x_0 - x)^2 + B(x_0 - x)^4.$$

In the close vicinity of the facet itself the crystal profile shape was indicated by inverse logarithmic derivative plot to correspond to a critical dependence given by Eq. (7), with  $\theta = 1.082 \pm 0.004$  obtained from direct data fit (Fig. 8).

#### 4. Discussion

We focus again on the region in which our crystal profile is extremely well described using critical dependence (7) with the value of critical exponent  $\theta = 1.499 \pm 0.003$  corresponding with great accuracy to the theoretically predicted value of  $\frac{3}{2}$  (characteristic for the Pokrovsky–Talapov–Gruber–Mullins universality class). Comparison of Eqs. (7) and (6) allows determination of the values of  $\beta_0$ ,  $\beta_1$  and  $\beta_3$  coefficients (bearing in mind that Eq. (6) describes the profile of a crystal within the coordinate frame with origin at the centre of the crystal):

$$\beta_0 = \lambda(z_c - z_{\text{facet}}),$$

$z_{\text{facet}} = 0$ , the facet itself being coincident with the  $x$ -axis of our data,

$$\beta_1 = \lambda(x_c - x_0),$$

$x_0$  taken as the facet edge position obtained from the critical fit in the stepped region,

$$\beta_3 = \lambda \frac{4}{27} \frac{1}{A^2},$$

$A$  from the critical fit in the stepped region.

An approximate value of the scaling parameter  $\lambda$  (Lagrange multiplier of Eq. (2)) can be estimated from the theoretical value  $f_0$  of the surface free energy per unit area of the flat facet, in the

expression [2] for the universal jump in surface curvature at  $T_R$ , where from

$$f_0 = \frac{\pi k_B T_R}{2 d^2},$$

where  $d$  is the distance between (111) lattice planes,  $d_{\text{Cu}_{2-x}\text{Se}}^{111} = 3.5 \times 10^{-10}$  m,  $T_R \approx 830$  K. We thus obtain  $f_0 \approx 161$  erg cm $^{-2}$ .

Using this value for  $\beta_0$  of our crystal grown 30 K below the roughening temperature ( $0.96 T_R$ ), we have an approximate working value  $\lambda \approx 418.39$  erg cm $^{-3}$ . Relying upon the results of fitting the profile data points to a circle  $z = z_c \pm \sqrt{R^2 - (x_c - x)^2}$  (in the region farthest away from the facet) for the values of  $x_c$ ,  $z_c$  (describing the position of the crystal centre within the coordinate frame of our data), we have:

$$\beta_0 \approx 161 \text{ erg cm}^{-2}, \quad \beta_1 \approx 25 \text{ erg cm}^{-2},$$

$$\beta_3 \approx 74 \text{ erg cm}^{-2}.$$

Restricting ourselves to experimental data fitting parameters only, we can state the values of ratios of coefficients in the stepped region of the crystal surface profile,

$$\frac{\beta_3}{\beta_0} = 0.46, \quad \frac{\beta_3}{\beta_1} = 3.0,$$

$$\frac{\beta_1}{\beta_0} = 0.15 \quad (\text{for Cu–Se}).$$

On few  $\mu\text{m}$  large Pb crystals [32] observed by STM after annealing at 440–560 K and cooling to room temperature, the critical exponent varies periodically with azimuth between 1.4 and 1.7 (reflecting the threefold symmetry of facet shape).

The values of coefficients obtained for the azimuth angle at which the  $\frac{3}{2}$ -critical dependence is approximately valid [32] are:

$$\beta_0 \approx 608.8 \text{ erg cm}^{-2}, \quad \beta_1 \approx 127.05 \text{ erg cm}^{-2}$$

$$\beta_3 \approx 126.57 \text{ erg cm}^{-2},$$

giving ratios

$$\frac{\beta_3}{\beta_0} = 0.21, \quad \frac{\beta_3}{\beta_1} = 1.00, \quad \frac{\beta_1}{\beta_0} = 0.21 \quad (\text{for Pb}).$$

The same crystals measured by STM in situ at the equilibration temperature of 380 K [5] have

circular facets, the critical exponent is no longer azimuth dependent and has an average value of  $1.49 \pm 0.06$ . Such contrast to the previous report of non-universal behaviour is explained as resulting from the crystal shape changes that apparently occur during cooling of the samples.

For small Si 3-D crystals [11] observed by SEM ex situ after equilibrating at  $900^\circ\text{C}$  the mean value of the ratio  $\beta_3/\beta_0 = 0.36 \pm 0.09$  was found, while for 2-D samples observed by TEM and REM in situ at  $900^\circ\text{C}$  the value of  $\beta_3/\beta_0 = 0.426$  was obtained. In both cases the profile is compatible with  $\frac{3}{2}$  power law within the tilt angle range  $3\text{--}17^\circ$ , while at small angles ( $0\text{--}1.5^\circ$ ) “no physically reasonable law can be assigned to the profile”.

Helium crystals have been the most extensively investigated ECS material thus far, both theoretically and experimentally. For HCP  $^4\text{He}(0001)$  facet, with  $T_R = 1.28\text{ K}$  and  $d_{\text{He}}^{0001} = 2.99 \times 10^{-10}\text{ m}$ , using the relation [2] for universal jump in surface curvature (or Fisher and Weeks [33] relation connecting the roughening temperature and principal surface stiffnesses at  $T_R$ ), the value of  $\beta_0$  should be  $0.31\text{ erg cm}^{-2}$ . As discussed in Ref. [34], the precise measurements by Babkin et al. [35] showed that close to  $c$ -direction it raises up to about  $0.31\text{ erg cm}^{-2}$ , the exact theoretical value (confirming that it is indeed justified to use the theoretical value at the roughening temperature in our estimate for  $\lambda$ ). The step energy found by Rolley et al. [24] is  $0.014 \pm 0.0005\text{ erg cm}^{-2}$  (falling off exponentially when approaching  $T_R$ , with a typical value of  $0.0002\text{ erg cm}^{-2}$  in the temperature range between  $1.13$  and  $1.232\text{ K}$  [34,36]). From the independent measurements of  $\gamma_{\parallel}$  component of surface stiffness (in the stepped surface region, for tilt angle  $< 1.3^\circ$ , where it is proportional to step interactions and vanishes linearly with tilt angle), the value of step interaction energy at  $0.1\text{ K}$  is deduced (see Figs. 3 and 4 in Ref. [37]) to be  $\approx 0.15\text{ erg cm}^{-2}$ . Keeping in mind that the values correspond to different temperatures below  $T_R$  we have

$$\begin{aligned} \beta_0 &= 0.31\text{ erg cm}^{-2}, & \beta_1 &= 0.014\text{ erg cm}^{-2}, \\ \beta_3 &\approx 0.15\text{ erg cm}^{-2}, \end{aligned}$$

which would give (indicative only) values of the ratios

$$\begin{aligned} \frac{\beta_3}{\beta_0} &\approx 0.48, & \frac{\beta_3}{\beta_1} &\approx 10.7, \\ \frac{\beta_1}{\beta_0} &\approx 0.045 & (\text{for } ^4\text{He}). \end{aligned}$$

As has already been pointed out the critical behaviour description of equilibrium crystal shape is appropriate in the stepped region only. The crossover angle between the stepped and the rough surface regions was predicted to be rather small in the case of helium where the crystal surfaces are weakly coupled to the underlying lattice. (The lattice potential is small and the solid–liquid interface thickness is much larger than the atomic spacing; thus the step height changes from 0 to  $a$  over a distance—step width—of several atomic spacings [24].) The opposite is expected in the case of metal–vacuum interface (surface) of metal crystals—the coupling should be strong, resulting in narrow, sharp steps, and thus enabling the stepped surface to extend to larger values of tilt angle  $\varphi$ .

The values of step interaction energy, step energy and facet surface free energy ratios obtained for cuprous selenide seem to fit pretty well within the overall framework—falling in between the values for metal (Pb) crystals and helium crystals at the opposite end—indicating a rather strong coupling. In agreement with that, our  $\theta = \frac{3}{2}$  fit extends up to  $\varphi \approx 17^\circ$ , comparable to  $13^\circ$  in Pb [1],  $15^\circ$  in In [9] and  $17^\circ$  in Si [11]. On the other hand, in  $^4\text{He}$ , the critical dependence describes the data up to  $0.1\text{ rad}$  ( $\approx 5.73^\circ$ ) [12], the other measurements showing that the crossover angle is even smaller [24,37]. Since both  $\beta_1$  and  $\beta_3$  are temperature dependent, further experimental data at different temperatures are necessary for a more detailed analysis.

The problem of the extent (angular range) of the  $\theta = \frac{3}{2}$  fit near the facet edge is far from being cleared in various materials. This has proved to be an experimentally difficult problem itself, for obvious reasons such as small sample sizes (of a few  $\mu\text{m}$  in most cases), scarcity of available data points in the region of interest and limited resolution. Besides, there seems to be an intrinsically

different behaviour that has often been noticed there, either directly or indirectly (through change in value of critical exponent of the stepped region when taking into account more and more points approaching the facet edge).

Rottman et al. [1] showed on a 9  $\mu\text{m}$  equilibrium Pb crystal, by choosing a number of different windows ( $\sim 0.8 \mu\text{m}$  wide) and determining within each of them the value of the critical exponent, that the effective value of  $\theta$  indeed had a minimum ( $\theta = 1.53$ ) within the “true critical region” between  $4^\circ$  and  $13^\circ$  from the edge. Extending the fitted data window to either side caused rising of the  $\theta$  values determined from the fit.

On small Pb single crystals with threefold facet shape symmetry [32] observed at room temperature, there was also pronounced dependence [38] on the fitting range  $\Delta r/r_f = 0.20\text{--}0.55$  ( $r_f$  is facet radius,  $\Delta r$  is fitting interval). The fit interval begins at the edge position, and the critical exponent value diminishes in general when taking into consideration more points away from the facet.

Métois and Heyraud [9] analysed equilibrium shape profiles of two In single crystals ( $\sim 4 \mu\text{m}$  in diameter), in the vicinity of a  $\{111\}$  facet. Their results show that the data in the region from  $0^\circ$  to  $\sim 5^\circ$  (with respect to facet orientation) are best described with the exponent  $\theta \approx 2$ , and from  $5^\circ$  to  $15^\circ$  with the exponent  $\theta \approx 1.60 \pm 0.10$ .

Elbaum [15] studied curvature jump of single crystals of ordinary  $\text{H}_2\text{O}$  ice grown from vapour by interference microscope. During in situ measurements, the sample was growing at a rate of  $\sim 50 \text{ \AA s}^{-1}$ , which had strong effect on the profile at temperatures farther below  $T_R$ . Just below  $T_R$  ( $\sim 271.81 \text{ K}$  in cooling), the surface profile shown contains the facet ( $2r \sim 0.3 \text{ mm}$ ) and a small range of surface orientations from  $0^\circ$  to  $\sim 1.3^\circ$  with respect to the facet. About 20 data points from this range gave exponent  $\theta = 1.74$ , fitted over the entire range. The authors conclude that the shape of the critical region is suggestive of Pokrovsky–Talapov transition, though an experiment in which the equilibrium would be reached, farther below the roughening temperature, is called for.

Carmi et al. [12] investigated the profile of HCP  $^4\text{He}$  crystals next to  $c$  facets (0001). The crystals of lateral dimensions as large as a few millimetres

were observed in situ at temperature stabilized below  $T_R$  (1.28 K) to an accuracy of 0.002 K. The authors claim that although their crystals were possibly not in global equilibrium, after equilibration times of the order of 10 min, the vicinal surfaces of interest should be in local equilibrium (since they should equilibrate as a rough surface, i.e., with time constants shorter than 20 s). In contrast to results on 9  $\mu\text{m}$  Pb crystals [1], the extent of fit interval on large  $^4\text{He}$  crystals was not limited to a “window”. The fitting function describes the data beginning from the chosen facet end position up to 0.1 rad ( $\approx 5.73^\circ$ ) with respect to the facet orientation. The obtained values of  $\theta$  from 13 photographs at various temperatures range from 1.49 to 1.65, giving the overall result  $\theta = 1.55 \pm 0.06$ .

All these observations seem to indicate that in situ measurements of non-growing, equilibrated crystals show better agreement with predicted value  $\theta = \frac{3}{2}$ , all the way to the facet edge (fit interval not being limited to a “window”).

In the case of cuprous selenide, application of inverse logarithmic derivative enabled us to clearly see the distinction between the stepped region behaviour (with  $\theta = 1.499$ ) and the different dependence near the facet edge, where an intriguing value of  $\theta = 1.082$  emerges. As the shape of our crystals was analysed on single crystals obtained by interrupting the crystal growth and cooling them rapidly to room temperature, one is tempted to say that such critical exponent value could rather be the result of (local) shape change that occurred during the cooling, than some new intrinsic behaviour.

However, during the growth [19,20,39] of our spherical  $\text{Cu}_{2-x}\text{Se}$  single crystals under conditions of constant volume growth rate, the exponential-like shape relaxation (the ratio of facet radius to sphere radius) towards the equilibrium form is observed. The other effect superimposed to the relaxation behaviour is the facet size oscillations (of order of 20%) during growth [20]. These oscillations seem to be correlated with step-like behaviour of facet height ( $z_{\text{facet}}$ ) value in time, the period of increase in facet diameter corresponding to the constant value of  $z_{\text{facet}}$  and the period of decrease in facet diameter corresponding to the

increase of  $z_{\text{facet}}$  value. The process bears resemblance to “burst-like” growth mode reported [40] for  ${}^4\text{He}$  solid/liquid interface at 2 mK. These growth dynamics features surely do affect the crystal shape during gradual approach to ideal equilibrium form, especially in the immediate vicinity of facets. They seem to be present during crystal growth in such diverse systems as solid  ${}^4\text{He}$  and  $\text{Cu}_{2-x}\text{Se}$ , and could be recognised in the equilibration–relaxation process of small Pb crystallites after an abrupt change in temperature [41].

Thus, if we accept that the  $\theta = 1.082$  behaviour of our crystal profile in the immediate vicinity of the facet edge is of the dynamic origin, one would expect that in the case of non-growing, ideally equilibrated crystal, the same  $\theta = \frac{3}{2}$  critical behaviour would prevail in this region. In that case the  $\theta = \frac{3}{2}$  fit would be extending from the facet edge all the way up to  $\varphi \approx 17^\circ$ , in accordance with predictions. (Note that the observed facet radius  $x_c - x_0 = 0.6934$  mm of the crystal analysed here is  $\approx 18\%$  larger than the facet radius  $x_c - x_0 = 0.5882$  mm that comes out as the fitting parameter from the  $\theta = 1.499$  critical behaviour in the stepped region. Seemingly, the sample was “quenched” in the growing part of the facet size oscillation cycle.)

Using the hereby established reliable, high-resolution method of crystal shape analysis (giving intervals of different behaviour and values of  $\theta$  and  $x_0$  independently), one should try observing the crystal shape in situ during growth and correlating it with simultaneous observations of growth dynamics features as the equilibrium form is approached.

## References

- [1] C. Rottman, M. Wortis, J.C. Heyraud, J.J. Métois, Phys. Rev. Lett. 52 (12) (1984) 1009.
- [2] C. Jayaprakash, W.F. Saam, S. Teitel, Phys. Rev. Lett. 50 (25) (1983) 2017.
- [3] J. Sáenz, N. García, Surf. Sci. 155 (1985) 24 and references therein.
- [4] J.J. Métois, J.C. Heyraud, Ultramicroscopy 31 (1989) 73.
- [5] H.P. Bonzel, Progr. Surf. Sci. 67 (2001) 45.
- [6] J.C. Heyraud, J.J. Métois, J. Crystal Growth 50 (1980) 571.
- [7] J.C. Heyraud, J.J. Métois, Acta Metall. 28 (1980) 1789.
- [8] J.C. Heyraud, J.J. Métois, Surf. Sci. 177 (1986) 213.
- [9] J.J. Métois, J.C. Heyraud, Surf. Sci. 180 (1987) 647.
- [10] J.J. Métois, J.C. Heyraud, Ultramicroscopy 31 (1989) 73.
- [11] J.M. Bermond, J.J. Métois, J.C. Heyraud, F. Floret, Surf. Sci. 416 (1988) 430.
- [12] Y. Carmi, S.G. Lipson, E. Polturak, Phys. Rev. B 36 (1987) 1894.
- [13] A.V. Babkin, H. Alles, P.J. Hakonen, A.Ya. Parshin, J.P. Ruutu, J.P. Saramäki, Phys. Rev. Lett. 75 (18) (1995) 3324.
- [14] A.V. Babkin, H. Alles, P.J. Hakonen, J.P. Ruutu, J.P. Saramäki, A.Ya. Parshin, J. Low Temp. Phys. 101 (1995) 525.
- [15] M. Elbaum, Phys. Rev. Lett. 67 (21) (1991) 2982.
- [16] T. Ohachi, S. Imai, T. Tanaka, H. Yamai, I. Taniguchi, Solid State Ion. 28–30 (1988) 1160.
- [17] T. Ohachi, I. Taniguchi, J. Crystal Growth 65 (1983) 84.
- [18] T. Ohachi, I. Taniguchi, in: P. Vashishta, J.N. Mundy, G.K. Shenoy (Eds.), Fast Ion Transport in Solids, Elsevier North-Holland, Amsterdam, 1979, p. 597.
- [19] Z. Vučić, J. Gladić, J. Crystal Growth 205 (1999) 136.
- [20] Z. Vučić, J. Gladić, Fizika A (Zagreb) 9(1) (2000) 9 ([http://fizika.phy.hr/fizika\\_a/av00/a9p009.htm](http://fizika.phy.hr/fizika_a/av00/a9p009.htm)).
- [21] E.M. Lifshitz, L.P. Pitaevskii, Landau and Lifshitz Course of Theoretical Physics, Vol. 5, Statistical Physics, 3rd Edition, Part 1, Pergamon Press, Oxford, 1980.
- [22] M. Wortis, Equilibrium crystal shapes and interfacial phase transitions, in: R. Vanselow, R. Howe (Eds.), Chemistry and Physics of Solid Surfaces, Vol. 7, Springer, Berlin, 1980.
- [23] S. Balibar, C. Guthmann, E. Rolley, J. Phys. I France 3 (1993) 1475.
- [24] E. Rolley, C. Guthmann, E. Chevalier, S. Balibar, J. Low Temp. Phys. 99 (5/6) (1995) 851.
- [25] A.F. Andreev, Zh. Eksp. Teor. Fiz. 80 (1981) 2042.
- [26] V.L. Pokrovsky, A.L. Talapov, Phys. Rev. Lett. 42 (1979) 65.
- [27] E.E. Gruber, W.W. Mullins, J. Phys. Chem. Solids 28 (1961) 875.
- [28] T. Ohachi, I. Taniguchi, J. Crystal Growth 40 (1977) 109.
- [29] T. Ohachi, B.R. Pamplin, J. Crystal Growth 42 (1977) 592.
- [30] J.R. Parker, Algorithms for Image Processing and Computer Vision, Wiley Computer Publishing, Wiley, New York, Chichester, Brisbane, Toronto, Singapore, Weinheim, 1997.
- [31] W.H. Press, B.P. Flannery, S.A. Teukolsky, W.T. Vetterling, Numerical Recipes, The Art of Scientific Computing (FORTRAN), Cambridge University Press, Cambridge, New York, New Rochelle, Melbourne, Sidney, 1987, p. 523.
- [32] K. Arenhold, S. Surnev, H.P. Bonzel, P. Wynblatt, Surf. Sci. 424 (1999) 271.
- [33] D.S. Fisher, J.D. Weeks, Phys. Rev. Lett. 50 (1983) 1077.
- [34] F. Gallet, S. Balibar, E. Rolley, J. Physique 48 (1987) 369.
- [35] A.V. Babkin, D.B. Kopeliovich, A.Ya. Parshin, Zh. Eksp. Teor. Fiz. 89 (1985) 2288.

- [36] P.E. Wolf, F. Gallet, S. Balibar, E. Rolley, P. Nozières, *J. Phys.* 46 (1985) 1987.
- [37] E. Rolley, E. Chevalier, C. Guthmann, S. Balibar, *Phys. Rev. Lett.* 72 (6) (1994) 872.
- [38] K. Arenhold, S. Surnev, H.P. Bonzel, P. Wynblatt, *Surf. Sci.* 417 (1998) L1160.
- [39] Z. Vučić, D. Lovrić, J. Gladić, in preparation.
- [40] J.P. Ruutu, P.J. Hakonen, A.V. Babkin, A.Ya. Parshin, J.S. Penttilä, J.P. Saramäki, G. Tvalashvili, *Phys. Rev. Lett.* 76 (1996) 4187.
- [41] K. Thürmer, J.E. Reutt-Robey, E.D. Williams, M. Uwaha, A. Emundts, H.P. Bonzel, *Phys. Rev. Lett.* 87 (2001) 186102.